J Braz. Soc. Mech. Sci. Eng. (2015) 37:1001–1013
DOI 10.1007/s40430-014-0224-1

TECHNICAL PAPER

Identification of static surface form errors from cutting force distribution in flat-end milling processes

Mehmet Aydın · Mehmet Uçar · Abdulkadir Cengiz · Mustafa Kurt

Received: 17 January 2014 / Accepted: 11 July 2014 / Published online: 31 July 2014

Abstract This paper presents a new and practical process simulation method to analyze surface errors caused by deflections of statically flexible flat-end mills. Milling force and surface error models are established to predict the surface error in various cutting conditions. The milling forces are predicted from the mechanistic model extended using the force distribution determined with an effective calibration procedure carried out by experimentally dividing the cutting part of the end mill into discs. The surface errors are modeled by establishing an analytical relationship between bending moments and deflections by means of the cantilever beam theory. These features make the present method very practical and efficient. A set of computational studies and experiments is performed to validate the effectiveness of the presented method. Comparisons of the results obtained numerically and experimentally confirm that the method is capable of accurate prediction of milling forces and surface errors. Finally, this method can be effectively applied for identifying appropriate cutting conditions in flat-end milling.

Keywords Cutting tool deflection · Flat-end milling · Milling force · Surface error

Technical Editor: Alexandre Mendes Abrao.

M. Aydın (✉)
The Program of Mechanics, Vocational School of Higher Education, Bilecik Şeyh Edebali University, Campus of Gülümbe, 11210 Bilecik, Turkey
e-mail: mehmet.aydin@bilecik.edu.tr

M. Uçar
Department of Automotive Engineering, Faculty of Technology, Kocaeli University, Campus of Umuttepe, 41380 Kocaeli, Turkey

A. Cengiz
Department of Mechanical Education, Faculty of Technical Education, Kocaeli University, Campus of Umuttepe, 41380 Kocaeli, Turkey

M. Kurt
Department of Mechanical Engineering, Faculty of Technology, Marmara University, Campus of Göztepe, 34722 Istanbul, Turkey

1 Introduction

End milling is an extensively used machining process in manufacturing industry due to its versatility and efficiency. Despite the improvement of machining technology together with the development of cutting tools, end mills experience static deflections under periodically varying milling forces, which are passed as surface form errors to the machined surface. Tool deflection that occurs especially when the feedrate is increased in milling operations causes an axial variation of chip thickness and cutting radius. This axial variation is more important particularly at a large axial depth of cut and may considerably influence the chip load and cutting forces.

The static deflection of the tool is the main factor influencing the machined surface and non-negligible because the productivity or material removal rate is constrained by form errors produced by the tool deflection. Thus, tool deflections should be considered as important disturbance factors causing surface errors. A review of the literature shows that there have been some approaches of the static deflections of the tool causing the surface errors to improve form accuracy of the machined surface. One of the earliest studies on surface form errors was carried out by Kline et al. [1]. They formulated the surface form errors

caused by a statically flexible end mill. Later, considering the effect of the cutting system deflection feedback, Sutherland and DeVor [2] developed an experimental method for estimating the cutting forces and the surface errors in flexible end milling systems. Budak and Altintas [3] considered the surface errors caused by the deflection of the end mill that is modeled as a cantilever beam clamped to the collect with linear springs. Kim et al. [4] established the cutting force and the tool deflection models including the effect of the surface inclination to analyze the surface form error in three-axis ball-end milling. Ryu et al. [5] suggested a method for the form error prediction in side wall end milling considering tool setting error and machine tool stiffness including the deformation of tool clamping parts. To identify the defects of the surfaces, Larue and Anselmetti [6] presented a method which takes into account the time and cost constraints in flank milling of steels at traditional speeds. Wan and Zhang [7] developed a general approach to predict surface form errors in peripheral milling using finite element method. Dépincé and Hascoët [8] dealt with the prediction accuracy of the machined surface using a contact point method. Lee and Kim [9] presented an analytical model to predict the geometric characteristics of the side wall in cylindrical end milling. Liu and Jiang [10] modeled machining error flow for the multistage machining processes (MMPs) considering form features of the workpiece by means of a rigid-body kinematics method. Desai and Rao [11] proposed an approach to characterize the variation of surface error profiles in peripheral milling of straight and curved geometries.

As known, milling forces induce the tool deflections which may diminish the accuracy and surface quality of the workpiece. Therefore, the determination of the tool deflection involves precisely the modeling of the cutting forces that are applied on the tool during the end milling process. On the other hand, although various studies related to the tool deflection inducing surface form errors have been reported over the past years, there have not been any studies on a method including the effect of the cutting force distribution in the axial direction to determine surface errors by analyzing cutting forces, as can be also seen from the above literature. Hence, the cutting force distribution along the tool z axis should be taken into consideration to obtain the satisfactory results of the surface form errors, which are mainly caused by the tool deflections in the normal plane to the surface. This paper presents a new process simulation method including the effect of the cutting force distribution in the axial direction to predict surface form errors with integrated cutter deflection for the flat-end milling processes. The main contributions of the proposed method are listed as follows:

(1) Based on the presently extended mechanistic model, the authors calculated the milling forces using the cutting force distribution determined from calibration procedure easily implemented by establishing an effective experiment design.
(2) The surface form error is determined from the novel deflection model developed using the cantilever beam theory which allows a precise evaluation of the machined surface.

Consequently, the accuracy of the method is verified by comparing the calculated cutting forces and surface form errors with the measured values. The presented method can be effectively implemented to improve workpiece quality requirements or dimensional and geometric tolerances.

2 Analytical models

2.1 Mechanistic model of milling force

The mechanistic model is adopted to formulate analytically milling forces, presented by Budak and Altintas [3].

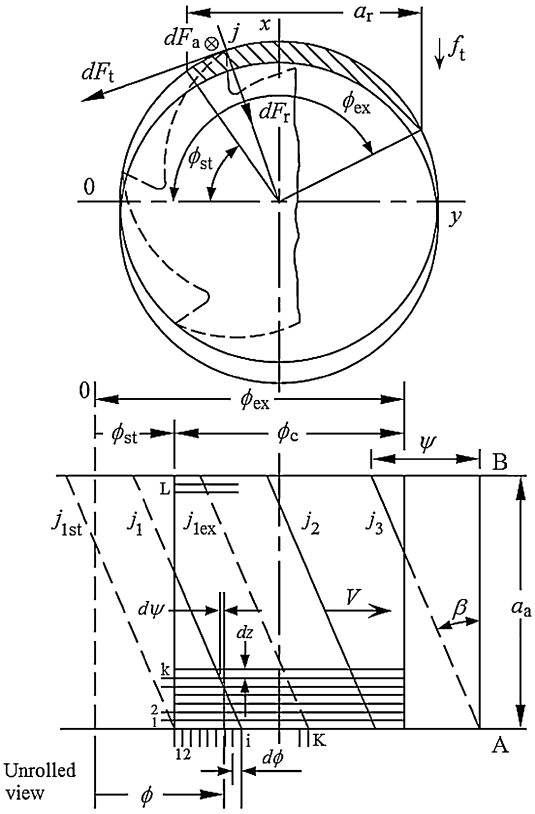

Fig. 1 Schematic diagram for computation of milling forces in end milling process [12]

Figure 1 shows the tangential, $dF_{t,j}$, radial, $dF_{r,j}$, and axial, $dF_{a,j}$, force components acting on element of the jth flute of a helical fluted end mill, whose elementary height is dz. The milling force components can be calculated from the undeformed chip thickness, $t_{c,j}(\phi_j(z))$, and cutting constants:

$$\left.\begin{aligned} dF_{t,j}(\phi,z) &= [k_t f_t \sin\phi_j(z)]\,dz,\\ dF_{r,j}(\phi,z) &= [k_r k_t f_t \sin\phi_j(z)]\,dz,\\ dF_{a,j}(\phi,z) &= [k_a k_t f_t \sin\phi_j(z)]\,dz, \end{aligned}\right\} \quad (1)$$

where f_t is the feed per tooth and $\phi_j(z)$ is the rotational angle of the jth flute, varying along the axial direction due to the helix angle, β. k_t, k_r and k_a are the cutting constants in tangential, radial and axial directions, respectively, and are generally described with exponential functions of the average undeformed chip thickness, $\bar{t}_c$, as follows:

$$k_t = c_t\left[\frac{f_t\int_{\phi_{st}}^{\phi_{ex}}\sin\phi\,d\phi}{\phi_{ex}-\phi_{st}}\right]^{-p_t},\quad k_r = c_r\left[\frac{f_t\int_{\phi_{st}}^{\phi_{ex}}\sin\phi\,d\phi}{\phi_{ex}-\phi_{st}}\right]^{-q_r},$$
$$k_a = c_a\left[\frac{f_t\int_{\phi_{st}}^{\phi_{ex}}\sin\phi\,d\phi}{\phi_{ex}-\phi_{st}}\right]^{-s_a}, \quad (2)$$

where ϕ is the tool rotational angle. c_t, c_r, c_a, p_t, q_r and s_a are obtained from the logarithmic variations of k_t, k_r and k_a with $\bar{t}_c$. ϕ_{st} and ϕ_{ex} are the start and exit cut angles, respectively.

2.1.1 *Identification of cutting constants with cutting force distribution method*

The accurate prediction of cutting forces is important in controlling the tool deflection and the machining accuracy [13]. The mechanistic model is commonly used for the calculation of milling forces. The measured average forces are modeled as concentrated forces for defining the cutting constants. However, the force intensities along the axial direction are non-uniformly distributed in helical milling since the chip thickness varies in the axial direction as the tool rotates.

For the identification of the cutting constants in this study, the helical fluted end mill modeled as a cantilever beam is experimentally sliced into equal N_z number of disc elements corresponding to plate elements of the workpiece in axial direction as shown in Fig. 2. For each disc element, the average forces, $\bar{F}_x$, $\bar{F}_y$ and $\bar{F}_z$, are measured from the specially devised half-immersion milling tests.

The experimentally determined force distribution can be described by quadratic equations. The least square method can be applied to regress a set of N_z pairs of experimental force data $(z_i, \bar{F}_{q,i})$ for $i \in \{1, 2, \ldots, N_z\}$ to a quadratic function, which is given by:

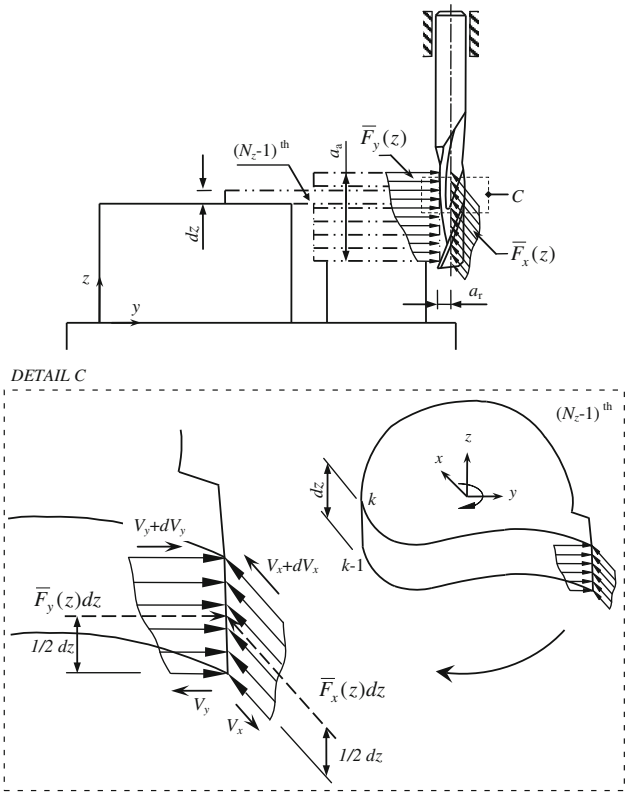

Fig. 2 End mill with chip load and free-body diagram of a disc element

$$f_q(z) = a_{q,0} + a_{q,1}\,z_i + a_{q,2}z_i^2 \quad (q = x, y, z), \quad (3)$$

where z_i is the axial position of disc elements. The value of z_i is taken as the axial position of the middle point of the disc element. $a_{q,0}$, $a_{q,1}$ and $a_{q,2}$ are the coefficients of polynomials.

As seen in Fig. 2, the distribution of milling forces along the end mill z axis can be represented by plotting free-body diagram of a disc element of length dz. Since the disc element has a small length, the distributed force can be considered as a uniformly distributed force with constant magnitude $\bar{F}_q(z)$ over the length dz. The distributed force is replaced by its resultant $\bar{F}_q(z)\,dz$. The shear force at the position $k-1$ is denoted by $V_q(z)$. Proceeding to the position k, the shear force is changed to the value $V_q(z) + (dV_q(z)/dz)\,dz$. The equilibrium equation of the element can be written as:

$$V_q(z) + \frac{dV_q(z)}{dz}dz = V_q(z) - \bar{F}_q(z)\,dz. \quad (4)$$

Integrating $dV_q(z) = -\bar{F}_q(z)\,dz$ on an elementary length dz to quantitatively determine the shear force for a force $\bar{F}_q(z)$ is expressed as follows:

$$V_{q,k} - V_{q,k-1} = -\int_{k-1}^{k}\bar{F}_q\,dz. \quad (5)$$

For the axial depth of cut, a_a, the shear force is determined by integrating $f_q(z)$ as follows:

$$V_q = -\int_0^{a_a} f_q(z)\,dz. \tag{6}$$

The tangential, radial and axial forces given by Eq. (1) are expressed through orthogonal transformation in the Cartesian coordinate system. The forces acting on the jth flute are then obtained from the integration of the intensities along the in cut part of the whole flute.

The total instantaneous milling forces acting on the tool at rotational angle ϕ are calculated from the numerical sum of milling forces generated by all flutes. For an end mill with N number of flutes, F_x, F_y and F_z are given by:

$$\left.\begin{aligned} F_x(\phi) &= \sum_{j=0}^{N-1}\left\{-k_t\frac{f_t}{2}\int_{z_{j,k-1}(\phi)}^{z_{j,k}(\phi)}[\sin 2\phi_j(z) + k_r(1-\cos 2\phi_j(z))]\right\}dz,\\ F_y(\phi) &= \sum_{j=0}^{N-1}\left\{k_t\frac{f_t}{2}\int_{z_{j,k-1}(\phi)}^{z_{j,k}(\phi)}[(1-\cos 2\phi_j(z)) - k_r\sin 2\phi_j(z))]\right\}dz,\\ F_z(\phi) &= \sum_{j=0}^{N-1}\left\{k_t\,k_a f_t\int_{z_{j,k-1}(\phi)}^{z_{j,k}(\phi)}[\sin\phi_j(z)]\right\}dz, \end{aligned}\right\} \tag{7}$$

where $z_{j,k-1}(\phi)$ and $z_{j,k}(\phi)$ are the lower and upper axial integration boundaries of the cutting part of the jth flute.

Integrating the x, y and z force components acting on the jth flute over one revolution of the tool yields to the analytical equations of average milling forces per tooth period. Finally, the cutting constants are established by combining Eq. (6) with those equations as follows:

$$\begin{aligned} k_t^{up} &= -\frac{2\pi}{Na_a}\left[\frac{4V_x}{f_t(2+k_r\pi)}\right], \quad k_t^{down} = \frac{2\pi}{Na_a}\left[\frac{4V_x}{f_t(2-k_r\pi)}\right],\\ k_r^{up} &= \frac{\pi V_x + 2V_y}{2V_x - \pi V_y}, \quad k_r^{down} = -\frac{\pi V_x - 2V_y}{2V_x + \pi V_y},\\ k_a^{up} &= \frac{2\pi}{Na_a}\left[\frac{V_z}{f_t k_t}\right], \quad k_a^{down} = \frac{2\pi}{Na_a}\left[\frac{V_z}{f_t k_t}\right]. \end{aligned} \tag{8}$$

where k_p^{up} and k_p^{down} (p = t, r, a) are the established constants for up and down end milling, respectively.

2.2 Proposed surface error model for statically flexible end mill

The surface in end milling results from the cutting edge trajectory determined by tool deflection, rotational angle and feedrate. Depending on the cutting geometry, several contact points generating the surface exist along the helical flute when the cutting tool cuts the workpiece. If a flute's edge point P_1 at the bottom of the end mill is aligned with the normal y axis, the contact point P_1 climbs the contact point P_2 owing to the helix angle when the end mill is rotated by an angle of $d\phi$. The movement from P_1 to P_2 leads to the surface generation. In up-milling, the surface occurs at the entry ($\phi_{st} = 0$), while in down-milling at the exit ($\phi_{ex} = \pi$). Since the normal cutting force will not be zero at this instant, any deflection of the elastic end mill will produce a static form error in the direction normal to the finished workpiece surface [14]. Thus, it is necessary to consider tool deflections according to the rotational angle.

To calculate the surface form errors exactly, the helical fluted end mill is modeled as a statically flexible cantilever beam with a varying area moment of inertia installed to the spindle-tool system through collet and axially divided into N_z number of disc elements with equal length, $dz = a_a/N_z$. Figure 3 shows the static deflection model of the end mill with the effective length L. The normal force, $w_{y,j}(\phi_j(z)) = dF_{y,j}(\phi_j(z))/dz$, of the cutting edge of each axial element is modeled as uniform line force localized at the contact point between the tool and workpiece.

To determine the milled surface, the variation of the milling force is considered as a function of the tool rotational angle ϕ. In other words, the variation of tool-workpiece contact point, which has a position corresponding to the tool rotational angle ϕ, is taken into account. It is assumed that the collet rigidly clamps the tool. Hence, the stiffness of the collet is not taken into account.

The tool axis bends into a circular arc of radius ρ when the end mill is subjected to a milling force $w_{y,j}$ as shown in Fig. 3. The length of the end mill along the tool axis does not change. However, the bending moment and the curvature of the axis vary along the length of the end mill. In such a case, the moment–curvature relationship can be considered to develop an equation for the deflection at every contact point where the new surface is generated. Under the assumption that the material of the end mill remains linearly elastic, the relationship of bending moment, $M_{y,j}(\phi_j(z))$, and curvature of the tool axis, $1/\rho$, can be written as [15]:

$$\frac{1}{\rho} = \frac{M_{y,j}(\phi_j(z))}{EI}. \tag{9}$$

As seen in the Fig. 3, the bending moment at a point C may be expressed as:

$$M_{y,j}(\phi_j(z)) = -w_{y,j}(\phi_j(z))\,\langle z - z_{L,m}(\phi_j)\rangle^1. \tag{10}$$

Substituting Eq. (10) into Eq. (9) gives:

$$\frac{1}{\rho} = -\frac{w_{y,j}(\phi_j(z))\,\langle z - z_{L,m}(\phi_j)\rangle}{EI}. \tag{11}$$

From elementary calculus and analytical geometry, the curvature of the end mill curve at any point $P(y,z)$ can be reformed as:

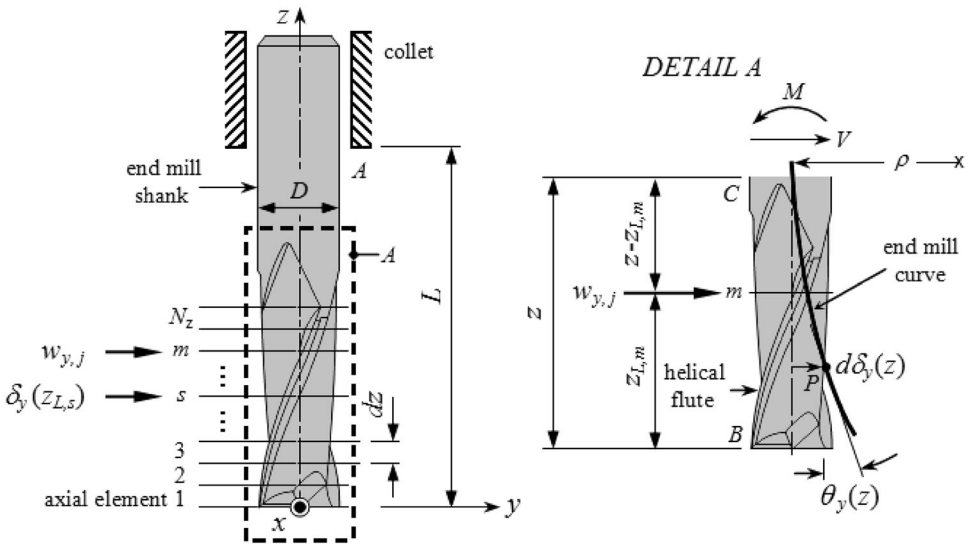

Fig. 3 Static deflection model of end mill

$$\frac{1}{\rho}=\frac{\frac{\mathrm{d}^2\delta_y(z)}{\mathrm{d}z^2}}{\left[1+\left(\frac{\mathrm{d}\delta_y(z)}{\mathrm{d}z}\right)^2\right]^{3/2}}, \tag{12}$$

where $\mathrm{d}\delta_y(z)/\mathrm{d}z$ and $\mathrm{d}^2\delta_y(z)/\mathrm{d}z^2$ are the first and second derivatives of the function $\delta_y(z)$, respectively. For small deflections, the slope $\mathrm{d}\delta_y(z)/\mathrm{d}z$ is very much small and its square $(\mathrm{d}\delta_y(z)/\mathrm{d}z)^2$ is negligible. Thus, Eq. (12) can be written as:

$$\frac{1}{\rho}=\frac{\mathrm{d}^2\delta_y(z)}{\mathrm{d}z^2}. \tag{13}$$

Substituting Eq. (11) into Eq. (13) and multiplying both members by $E\,I$ yield:

$$E\,I\frac{\mathrm{d}^2\delta_y(z)}{\mathrm{d}z^2}=-w_{y,j}(\phi_j(z))\ \langle z-z_{L,m}(\phi_j)\rangle^1. \tag{14}$$

Integration of Eq. (14) in z yields:

$$E\,I\ \frac{\mathrm{d}\delta_y(z)}{\mathrm{d}z}=-\int_0^z w_{y,j}(\phi_j(z))\ \langle z-z_{L,m}(\phi_j)\rangle^1\,\mathrm{d}z+C_{y,1}. \tag{15}$$

In the case of the cantilever beam, the slope at the fixed end A is zero. Letting $z=L$ and $\theta_y(z)=\mathrm{d}\delta_y(z)/\mathrm{d}z=0$ in Eq. (15), the integration constant $C_{y,1}$ can be determined as:

$$C_{y,1}=\frac{1}{2}w_{y,j}(\phi_j(z))\ [L-z_{L,m}(\phi_j)]^2.$$

Integrating both members of Eq. (15) in z is expressed as:

$$E\,I\ \delta_y(z)=-\int_0^z \mathrm{d}z\int_0^z w_{y,j}(\phi_j(z))\ \langle z-z_{L,m}(\phi_j)\rangle^1\,\mathrm{d}z + C_{y,1}\ z+C_{y,2}. \tag{16}$$

The deflection, $\delta_y(z)$, at the fixed end A is also zero. Replacing $z=L$ and the integration constant $C_{y,1}$ in Eq. (16) yields to the integration constant $C_{y,2}$:

$$C_{y,2}=-\frac{1}{6}w_{y,j}(\phi_j(z))\ [L-z_{L,m}(\phi_j)]^2\ [2L+z_{L,m}(\phi_j)].$$

Carrying the values of the integration constants $C_{y,1}$ and $C_{y,2}$ back into Eq. (16), the deflection $\delta_y(z_{L,s}(\varphi_j))$ of the end mill in the y direction at the contact point $z_{L,s}$ caused by the normal force in the mth element of the jth flute can be expressed as:

$$\delta_y(z_{L,s}(\phi_j))=\frac{w_{y,j}(\phi_j(z))}{6\,E\,I}\ \{-\langle v_s(\phi_j)-v_m(\phi_j)\rangle^3 + [L-v_m(\varphi_j)]^2\ [3\,v_s(\varphi_j)-2L-v_m(\varphi_j)]\}, \tag{17}$$

where E is the Young's modulus of the tool material, I is the moment of inertia of the tool cross section, L is the overhang, $v_s(\phi_j)=L-z\,(\phi_j)$ and $v_m(\phi_j)=L-z_{L,m}(\phi_j)$ are the positions of the deflection and the applied force from the fixed end A, respectively.

The geometrical model of a two-fluted end mill is established to determine the moment of inertia of the cross section of the end mill as proposed by Kivanc and Budak [16]. Figure 4 shows their geometrical parameters of the cross section of the end mill. The equivalent radius (R_{eq}) for the first tooth of a two-fluted end mill is determined for rotational angle ϕ from cosine law as follows:

$$R_{\mathrm{eq,\,two-fluted}}(\phi)=-a\ \cos(\phi)+\sqrt{(r^2-a^2)+a^2\cos^2(\phi)} \qquad 0<\phi\le\pi, \tag{18}$$

where r is the radius of the arc and a is the position of the center of the arc.

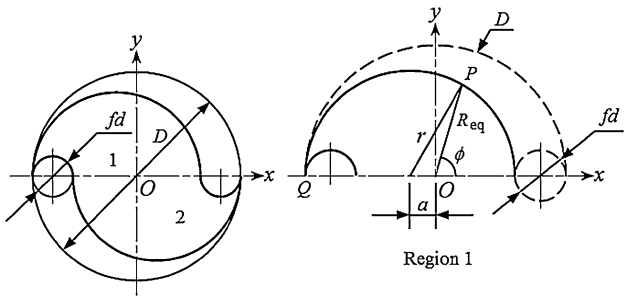

Fig. 4 Cross section of the two-fluted end mill

To determine analytically the moment of inertia of the whole cross section, the moment of inertia of the first tooth of a two-fluted end mill about x and y axes is found as follows:

$$\left.\begin{aligned} I_{x,\text{two-fluted}} &= \left[\int_0^{\pi}\int_0^{R_{\text{eq, two-fluted}}(\phi)} \Omega^3 \sin^2(\phi)\,\mathrm{d}\Omega\,\mathrm{d}\phi\right] \\ &\quad -\left[\frac{1}{8}\pi\left(\frac{fd}{2}\right)^4\right], \\ I_{y,\text{two-fluted}} &= \left[\int_0^{\pi}\int_0^{R_{\text{eq, two-fluted}}(\phi)} \Omega^3 \cos^2(\phi)\,\mathrm{d}\Omega\,\mathrm{d}\phi\right] \\ &\quad -\left[\frac{1}{8}\pi\left(\frac{fd}{2}\right)^4+\frac{\pi fd^2}{8}\left(r+a-\frac{fd}{2}\right)^2\right], \end{aligned}\right\} \tag{19}$$

where $0<\Omega\le R_{\text{eq}}(\phi)$. The total moment of inertia of the cross section is determined by multiplying that of the first tooth by the number of flutes, N, as follows:

$$\left.\begin{aligned} I_{x,\text{two-fluted, TOTAL}} &= N\,(I_{x,\text{two-fluted}}), \\ I_{y,\text{two-fluted, TOTAL}} &= N\,(I_{y,\text{two-fluted}}), \end{aligned}\right\} \tag{20}$$

where $I_{x,\text{two-fluted}}$ and $I_{y,\text{two-fluted}}$ are the moments of inertia of the end mill with respect to the principle axes x and y, respectively. The moment of inertia at every tool rotational angle varies along the axis of the end mill due to the helix angle. This means that the surface error also changes at each tool rotational angle due to the rigidity of the tool variation.

The total static deflection $\delta_y(z_{L,s})$ at axial contact point $z_{L,s}$ is computed from the sum of the elementary deflections generated by all elementary cutting edges engaged simultaneously in the workpiece:

$$\begin{aligned} \delta_y(z_{L,s}) &= \sum_{i=1}^{N_z}\int_{\phi_{\text{st}}}^{\phi_{\text{ex}}} \delta_{y,i}(z_{L,s}(\phi_j)) \\ &= \sum_{i=1}^{N_z}\left(\frac{1}{6\,E\,I}\int_{\phi_{\text{st}}}^{\phi_{\text{ex}}} M_{y,i}(\phi_j(z_{L,s}))\right) \end{aligned} \tag{21}$$

where the bending moment, $M_{y,i}(\varphi_j(z_{L,s}))$, is given by:

$$\begin{aligned} M_{y,i}(\phi_j(z_{L,s})) = w_{y,j}(\phi_j(z))\,\{&-\langle v_s(\phi_j)-v_m(\phi_j)\rangle^3 \\ &+[L-v_m(\phi_j)]^2\,[3\,v_s(\phi_j)-2L-v_m(\phi_j)]\}. \end{aligned}$$

At the points where the cutting edge is in contact with the milled surface, the tool deflection, $\delta_y(z_{L,s})$, in the normal direction is passed as a form error, $e_y(z_{L,s})$, to the milled surface. Consequently, the surface form error can be precisely predicted with the consideration of the tool deflection.

$$e_y(z_{L,s}) = \delta_y(z_{L,s}) \tag{22}$$

Since the milled surface results from the traces generated by the tool, the variation of the contact point is taken into account to predict the surface form. Thus, rotating the tool in angular increments $\mathrm{d}\phi$ over one flute passing period $2\pi/N$, the tool deflections are computed with respect to each angular position corresponding to the position of the contact point and superposed to determine the finish surface form.

3 Experimental procedures

3.1 Implementation of calibration tests

An effective experimental design method has been constructed for the calibration of the cutting constants. The method is based on the identification of the force distribution on the tool. Therefore, the end mill is experimentally divided into N_z number of discs along z axis, which is modeled as a cantilever beam. The machining specimens are the blocks composed of sheet metal slices. As seen in Fig. 5, one of the slices is rigidly attached to the dynamometer. The other slices are also fixed firmly on the machine table. At first, the tip point of the end mill is lower at a slight distance away from the slice on the dynamometer and the cutting forces acting on the first disc element are evaluated in this case. It should be noted that the forces are achieved from the slice on the dynamometer, while the side walls of the whole slices are machined during the experimental work. Measuring cutting forces acting on the disc element at the slice is performed by applying a space between the slice on the dynamometer and the other slices.

After measuring the cutting forces acting on the disc element at the first slice, the axial positions of the end mill and the slices on the worktable are changed to identify the cutting forces acting on each disc element. To adjust the axial position of the end mill, the machine head is moved downwards with increment of $\mathrm{d}z$. The axial positions of the slices on the worktable are also changed by placing them under the first slice, respectively. The tests are repeated until the cutting forces acting on the last disc element are measured. As a result of the tests, the force distribution is illustrated on the cutting tool modeled as a cantilever beam.

Based on the proposed method, a set of half-immersion up- and down-milling experiments has been carried out to

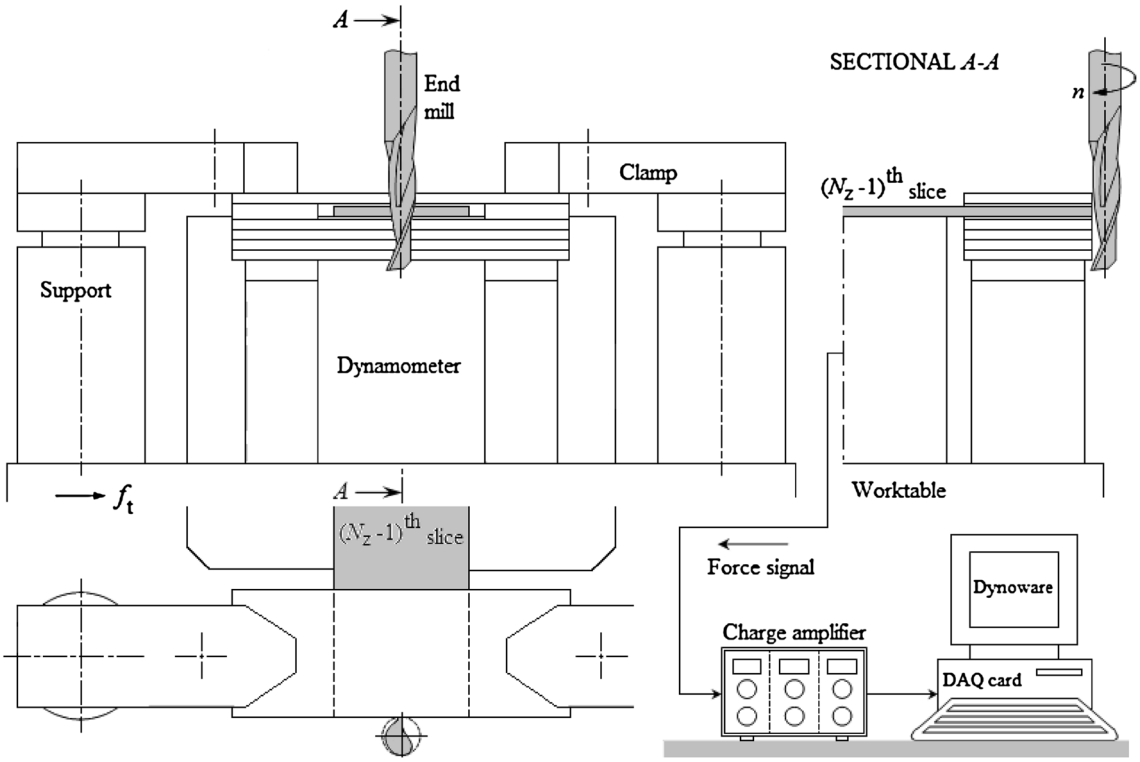

Fig. 5 Set-up for calibration tests

identify the cutting constants at varying feedrates with fixed cutting speed and the average values of cutting forces were determined at every feedrate. All experimental works were performed on a Johnford VCM-550 machining center. Single-fluted carbide flat-end mills with 30 degree (°) helix angle, normal rake angles of 5, 10, 15° and diameters of 8, 10, 12 mm were used in milling of aluminum alloy 7075-T651. The experiments were conducted in dry cutting conditions, at a fixed axial depth of cut one and a half times larger than the diameter of the tool, at a fixed cutting speed 30 m/min, at three different feed per tooth 0.04, 0.08, 0.12 mm/tooth. The feed, F_x, normal, F_y, and axial, F_z, forces were measured by a piezoelectric dynamometer, Kistler 9443B, a multi-channel charge amplifier, Kistler 5019B, and a data acquisition (DAQ) card, PCL-812PG. The force signals were displayed and recorded with a data acquisition program, DynoWare 2.31.

4 Simulation and experimental results

4.1 Cutting force distribution method results

To mechanistically establish the cutting constants which can make a proportional relationship between cutting forces and the undeformed chip thickness, the average cutting forces on all the disc elements were determined by experimentally dividing the cutting part of the end mill into N_z number of elementary discs. Figure 6 shows the variations of the cutting forces F_x and F_y along the cutting part of the end mill. It can be concluded that the cutting forces are distributed along the axial depth of cut and result in a parabolically varying force of intensity $f_q(z)$ in the end milling. The cutting force intensities are obtained increasing along the axial direction because immersion boundaries and chip thickness change continually during the milling

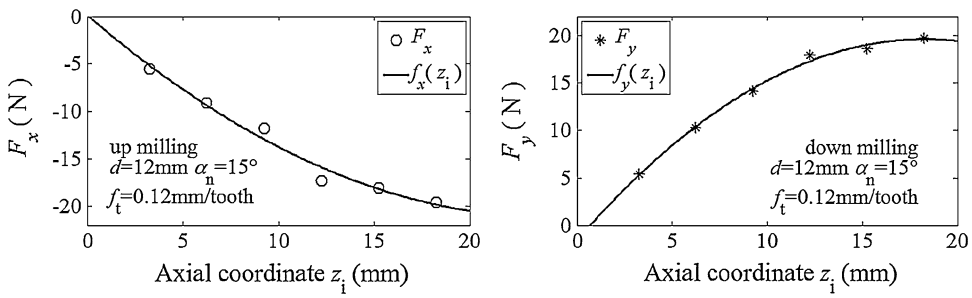

Fig. 6 Variations of cutting forces F_x and F_y along cutting part of end mill

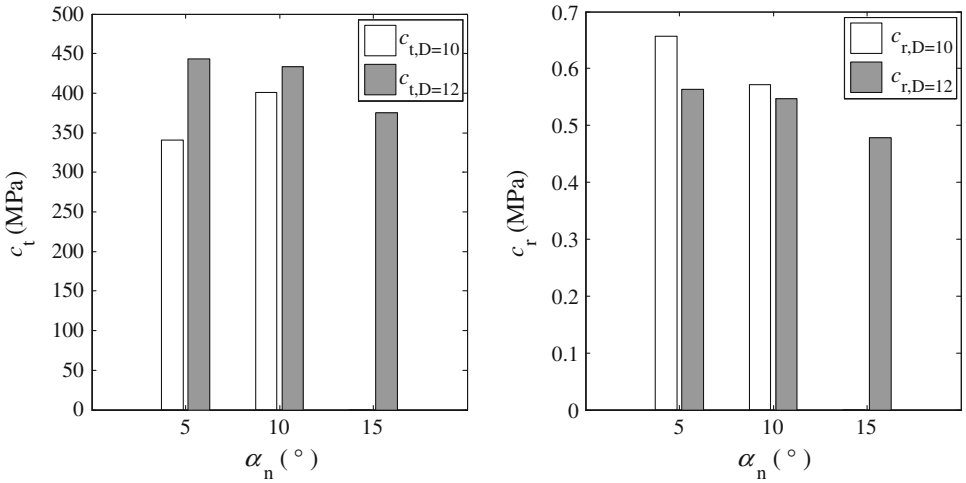

Fig. 7 Cutting constants c_t and c_r calibrated for up-milling process

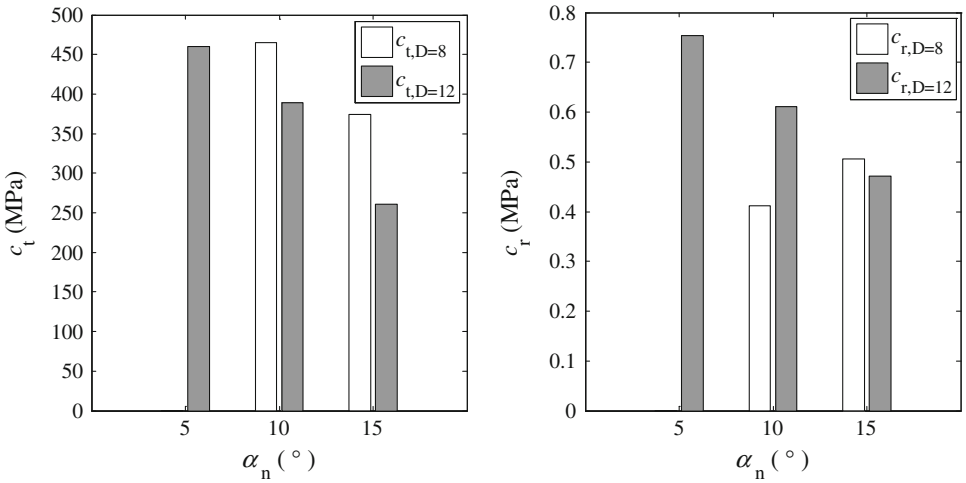

Fig. 8 Cutting constants c_t and c_r calibrated for down-milling process

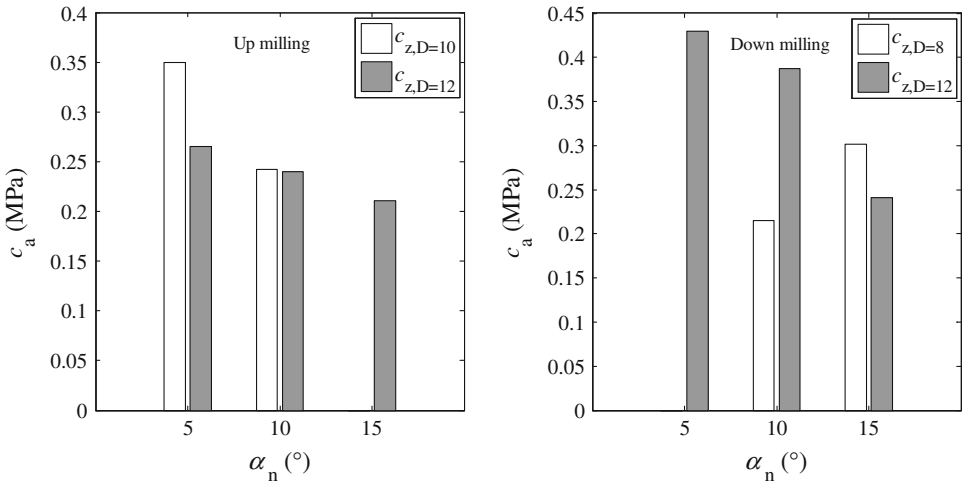

Fig. 9 Cutting constants c_a calibrated for up- and down-milling processes

process. The variation of the axial cutting force, F_z, is also similar to the feed, F_x, and normal, F_y, cutting forces. For the identification of the cutting constants, the variations are identified with polynomial equations of second degree. Subsequently, the shear forces are calculated from the cutting force polynomial equations using Eq. (6).

Table 1 The average milling forces measured and predicted from the proposed method

Test no	Cutting speed V (m/min)	Feed per tooth f_t (mm/tooth)	Milling type	Diameter D (mm)	Rake angle α_n (°)	Force direction	Measured force (N)	Predicted force, (N)	Absolute deviation ε (%)
1	30	0.04	Up	12	15	F_x	−130.6	−129.1	1.1
						F_y	277	270	2.5
						F_z	51.9	57	9.8
2	30	0.08	Up	12	15	F_x	−269.8	−258.1	4.3
						F_y	524.4	540	3
						F_z	106.5	113.9	6.9
3	30	0.12	Up	12	10	F_x	−570	−511.6	10.2
						F_y	948.5	935.3	1.4
						F_z	235.6	224.5	4.7
4	30	0.04	Down	12	5	F_x	−266.1	−249.7	6.2
						F_y	340.7	331.2	2.8
						F_z	−134.8	−142.4	5.6
5	30	0.08	Down	12	10	F_x	−395.9	−342.3	13.5
						F_y	536.3	560.2	4.5
						F_z	−203.2	−216.8	6.7
6	30	0.12	Down	12	5	F_x	−802	−749.2	6.6
						F_y	1004	993.6	1
						F_z	−487.7	−427.2	12.4
7	30	0.04	Up	10	10	F_x	−145.5	−137.4	5.6
						F_y	249.2	240.6	3.5
						F_z	56.9	58.2	2.3
8	30	0.08	Up	10	10	F_x	−277.7	−274.8	1
						F_y	465	481.2	3.5
						F_z	126.1	116.5	7.6
9	30	0.12	Up	10	5	F_x	−424.1	−403.3	4.9
						F_y	642.5	613.8	4.5
						F_z	205.5	214.8	4.5
10	30	0.04	Down	8	10	F_x	−103.7	−92	11.3
						F_y	223.4	223.2	0.1
						F_z	−42	−48	14.3
11	30	0.08	Down	8	15	F_x	−158.3	−181.3	14.5
						F_y	373	359	3.8
						F_z	−99.7	−108.4	8.7
12	30	0.12	Down	8	10	F_x	−311.6	−275.8	11.5
						F_y	648.1	669.6	3.3
						F_z	−131.2	−144	9.8

The cutting constants c_t, c_r and c_a are derived by substituting the calculated shear forces into Eq. (8). Figures 7, 8 and 9 show the cutting constants obtained as the exponential function of the average undeformed chip thickness from the proposed method for up- and down-milling processes. It should be noted that the calibrated constants based on the proposed method are given for not only tool-part couple but also tool diameter and milling type. In addition, the experiments cause different predictions of the constants, which are carried out in various machining conditions. The constants derived for 12 mm diameter end mills with three different rake angles are found decreasing with increasing rake angle in all cases of up- and down-milling, while such a tendency is not determined for end mills of 8 and 10 mm diameter.

4.2 Accuracy of milling force prediction

The accuracy of the milling force predictions was verified through the comparison of forces obtained from flat-end milling tests. The milling tests (half-immersion up- and down-milling) were carried out on aluminum alloy 7075-T651 thick blocks without coolant, at a constant cutting speed of 30 m/min, at three different feedrates of 0.04, 0.08, 0.12 mm/tooth and at a constant axial depth of cut of one-half of the tool diameter. The cutting tools were two-fluted carbide end mills with 30° helix angle, three different rake angles 5, 10, 15° and three different diameters 8, 10, and 12 mm.

Table 1 lists the performance of the average milling force predictions identified mechanistically from the proposed method. From the results given in the table, the mean absolute deviations of the predicted F_x, F_y and F_z values are found as 7.6, 2.8 and 7.8 %, respectively. That is, their prediction accuracies are 92.4, 97.2 and 92.2 %, respectively. The predicted maximum F_x value also has the mean absolute deviation lesser than 10 %. However, the mean absolute deviation is slightly more than 10 % for the predicted maximum F_y value and found to be <15 % for the predicted maximum F_z value. It can be concluded that the proposed method provides an excellent accuracy rate for the prediction of milling forces. On the other hand, the deviations between the predicted and measured force values can be attributed to the effects of cutting tool deflection. The other reason for the deviations may be the small amplitude fluctuations of the forces produced by cutting tool, workpiece and dynamometer vibrations.

The predicted and measured instantaneous force profiles are also considered to see the effectiveness of the proposed method. Figures 10 and 11 shows the simulated and measured force variations of half-immersion up- and down-milling test examples for one-half tool revolutions, respectively. It can be seen that the agreement between the experimental forces and the force predictions based on the constants identified mechanistically from the half-immersion milling tests is quite satisfactory. Thus, the proposed method is able to predict milling force components with a satisfactory accuracy.

4.3 Accuracy of surface error prediction

A series of half-immersion up- and down-milling experiments was considered to validate the accuracy and the effectiveness of the presently proposed model by comparing the simulation results with the experimental results. The experimental instruments and conditions were the same as milling force measurements. The milled surface errors were measured from the intended reference surface along axial direction using a coordinate measuring

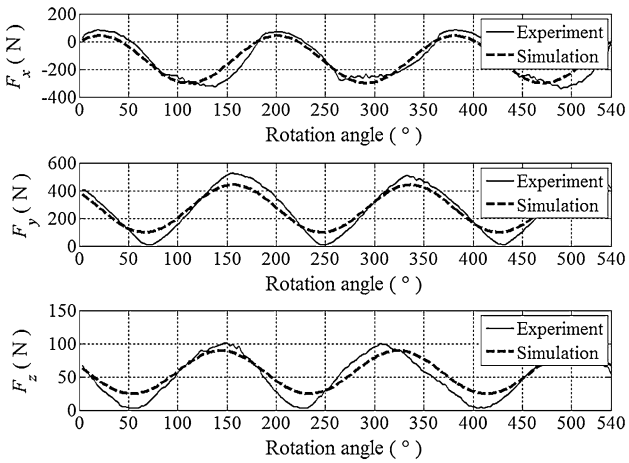

Fig. 10 Milling forces measured and predicted from the proposed method for a half-immersion up-milling ($D = 12$ mm, $\alpha_n = 15°$, $V = 30$ m/min, $f_t = 0.04$ mm/tooth, $a_a = 18$ mm)

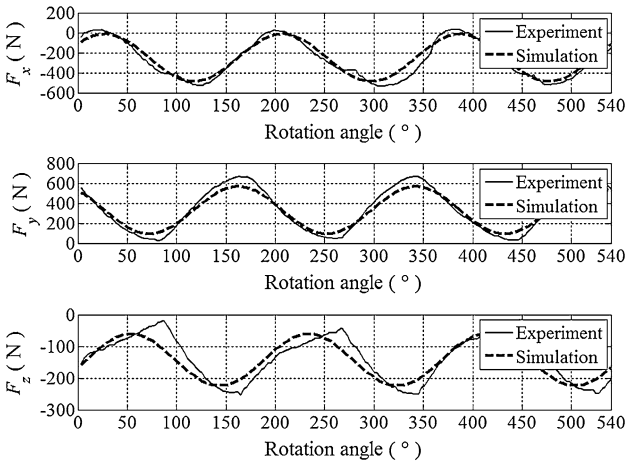

Fig. 11 Milling forces measured and predicted from the proposed method for a half-immersion down-milling ($D = 12$ mm, $\alpha_n = 5°$, $V = 30$ m/min, $f_t = 0.04$ mm/tooth, $a_a = 18$ mm)

machine. The measured value of each axial position was subtracted from radial depth of cut (a_r) to obtain surface form error.

Figures 12 and 13 shows surface error profiles of half-immersion up- and down-milling test examples predicted by the present simulation model and measured by experiment, respectively. These graphs represent the surface error values at different axial position from the top of the workpiece to the bottom. The surface errors increase approximately in a linear manner as the axial depth position is further away from the cantilever tip of the helical end mill. As can be observed from the figures, the simulated surface error distributions considering the static deflection of the tool by the present model are very similar and close to the experimentally measured surface profiles in both shape and magnitude. This shows that the improved

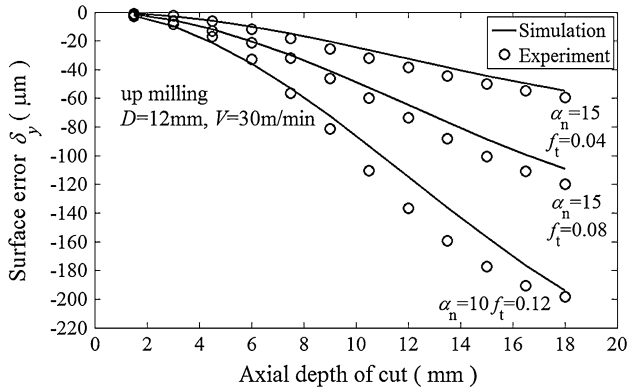

Fig. 12 Profile curves of predicted and measured surface form error for half-immersion up-milling

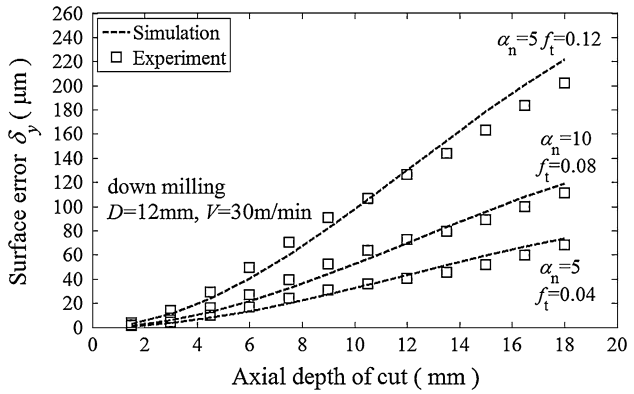

Fig. 13 Profile curves of predicted and measured surface form error for half-immersion down-milling

model can predict the surface finish with satisfactory accuracy.

Figures 14 and 15 schematize the milled profiles obtained on the surface of the workpiece and the chip load variation in the up-milling and down-milling processes, respectively. P_1 and P_2 are contact points corresponding to the tool's angular position. The surface of the workpiece is divided into P_{Nz} points: P_i, $i \in 1, 2, \ldots, N_z$. As the tool turns with an angular increment of $d\phi$, cutting edge reaches from the start position to the maximum chip load position. In this case, the surface form error occurs due to the tool deflection on the surface generation line.

As seen in the Figs. 14 and 15, the surface generation is not the same for up-milling and down-milling. In the case of up-milling, the cutting teeth enter in the workpiece and cause an overcutting form error since the cutting forces deflect the cutting tool towards the workpiece surface. In down-milling process, the normal cutting forces acting on the cutting tool push it out of the workpiece, therefore resulting in an undercutting form error. In the case of up-milling, because the cutting tool is pushed into the workpiece which withstands the deflection, the surface error

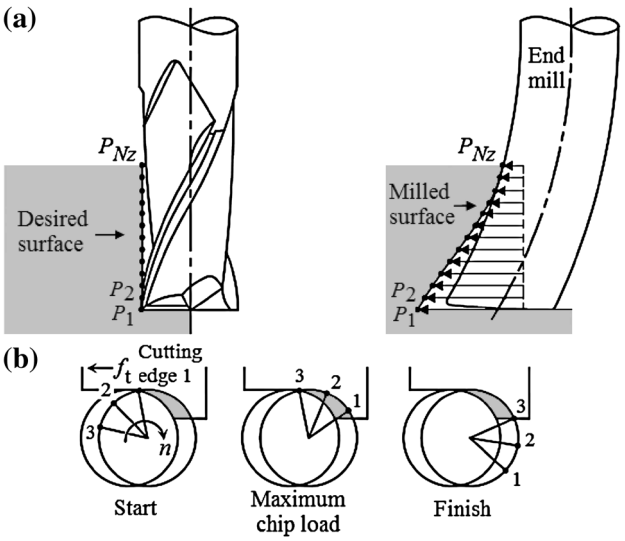

Fig. 14 Surface generation in up-milling: **a** milled surface, **b** chip load variation

magnitudes are less than down-milling. As the cutting tool

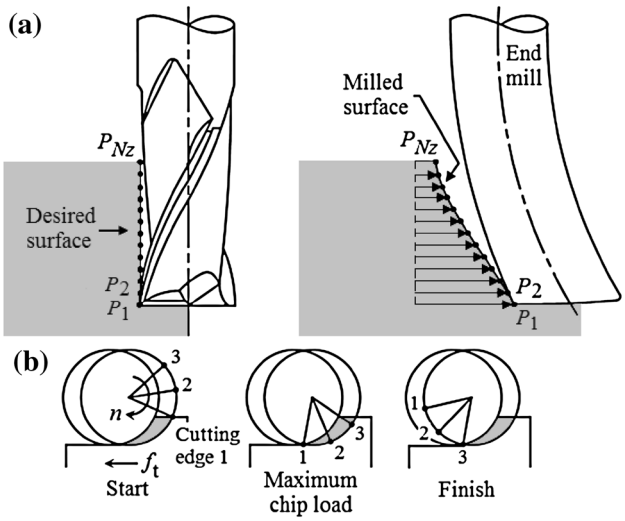

Fig. 15 Surface generation in down-milling: **a** milled surface, **b** chip load variation

deflects away from the workpiece in down-milling, there is not opposing contact rigidity.

In Table 2, the measured error values at the bottom of the workpiece are summarized and compared with their predicted counterparts. The maximum difference between the predicted and the measured surface error values is lesser than 10 % in all the cases. In other words, the predicted errors are very close to the measured ones. It can be concluded that the proposed method is quite effective for process planning of end milling operations. On the other hand, the difference between the measured and the predicted error values may be attributed to unstable cutting

Table 2 Comparison of surface errors predicted and measured at the bottom of the workpiece

Test no	Cutting speed V (m/min)	Feed per tooth f_t (mm/tooth)	Milling type	Diameter D (mm)	Rake angle α_n (°)	Overhang L (mm)	Measured surface error (μm)	Predicted surface error (μm)	Deviation ε (%)
1	30	0.04	Up	12	15	48	−59.3	−54.6	7.9
2	30	0.08	Up	12	15	48	−120	−109.1	9.1
3	30	0.12	Up	12	10	48	−198.5	−193.9	2.3
4	30	0.04	Down	12	5	48	68	73.9	8.7
5	30	0.08	Down	12	10	48	111.3	118.9	6.8
6	30	0.12	Down	12	5	48	202.1	221.6	9.6
7	30	0.04	Up	10	10	36	−57	−52.4	8.1
8	30	0.08	Up	10	10	36	−111	−104.7	5.7
9	30	0.12	Up	10	5	36	−151	−137.5	8.9
10	30	0.04	Down	8	10	32	45	47.9	6.4
11	30	0.08	Down	8	15	32	73.5	79.5	8.2
12	30	0.12	Down	8	10	32	134.3	143.7	7.0
Mean absolute deviation									7.4

action near the tool end such as rubbing and unstable removal of the chip.

The dimensional surface error model in Ref. [3] is also investigated to evaluate the efficiency of the improved simulation model. The model in Ref. [3], based on the average force approach, does not take into account the influence of the cutting force distribution in the axial direction on surface errors. However, the presently suggested model includes the effect of the cutting force distribution to identify the surface errors. Comparing the surface error model presented here to the model in Ref. [3], it is found that the surface profiles simulated using the improved model are similar in shape to the ones obtained from the model in Ref. [3] for up-milling. Although surface profiles predicted using the proposed model approximately linearly vary in down-milling, the profiles nearly remain constant along y axis in the model in Ref. [3]. The greatest discrepancy between the measured and predicted dimensional surface errors is about 15 % for both up- and down-milling operations in the model in Ref. [3]. The greatest discrepancy between the surface error values measured and predicted from the improved model is <10 %, as seen in Table 2. Finally, the surface error model based on the force distribution is more effective than the one dependent on the average force.

5 Conclusions

In this study, a process simulation method including the effect of the cutting force distribution in the axial direction has been suggested for analytical prediction of surface form errors in the flat-end milling processes. This model is composed of two parts: milling force model and surface form error model. The first contribution of this method is that the milling forces are predicted from the mechanistic model extended by experimentally considering the force distribution along the cutting part of the end mill by means of the presented calibration procedure. The helical fluted end mill is represented by a cantilever beam, which can accurately model the geometry of the tool. Its other contribution is that static tool deflections are calculated from a new and efficient model established using the cantilever beam theory. The form errors remaining on the surface are directly predicted from the tool deflection and compared with the experimental results. It can be seen from the results that the improved models allow satisfactory computational results of cutting forces and surface form errors in the flat-end milling processes. The model can help process planners in determining the cutting process conditions and the operation planning so that the milled surface approaches the nominal form as much as possible.

Acknowledgments This research is financially supported by Scientific Research Projects Coordinators of Kocaeli University in Turkey (Project Code: 2012/07). This support is greatly appreciated. The authors are also grateful to the Department of Mechanical Education, Marmara University, İstanbul, Turkey, for providing the laboratory facilities to carry out the experimental tests.

References

1. Kline WA, DeVor RE, Shareef IA (1982) The prediction of surface accuracy in end milling. J Eng Ind Trans ASME 104:272–278
2. Sutherland JW, DeVor RE (1986) An improved method for cutting force and surface error prediction in flexible end milling systems. J Eng Ind Trans ASME 108:269–279

3. Budak E, Altintas Y (1994) Peripheral milling conditions for improved dimensional accuracy. Int J Mach Tools Manuf 34:907–918
4. Kim GM, Kim BH, Chu CN (2003) Estimation of cutter deflection and form error in ball-end milling processes. Int J Mach Tools Manuf 43:917–924
5. Ryu SH, Lee HS, Chu CN (2003) The form error prediction in side wall machining considering tool deflection. Int J Mach Tools Manuf 43:1405–1411
6. Larue A, Anselmetti B (2003) Deviation of a machined surface in flank milling. Int J Mach Tools Manuf 43:129–138
7. Wan M, Zhang WH (2006) Efficient algorithms for calculations of static form errors in peripheral milling. J Mater Process Tech 171:156–165
8. Dépincé P, Hascoët JY (2006) Active integration of tool deflection effects in end milling. Part I: prediction of milled surfaces. Int J Mach Tools Manuf 46:937–944
9. Lee KS, Kim K (2008) Unavoidable geometric errors in the side walls of end-milled parts-cylindrical surface. J Mech Sci Technol 22:522–531
10. Liu D, Jiang P (2009) Modelling of machining error flow based on form features for multistage processes. Int J Comput Integr Manuf 22:857–876
11. Desai KA, Rao PVM (2012) On cutter deflection surface errors in peripheral milling. J Mater Process Technol 212:2443–2454
12. Tlusty G (2000) Manufacturing process and equipment. Prentice Hall, New Jersey
13. Liu XW, Cheng K, Webb D, Luo XC (2002) Improved dynamic cutting force model in peripheral milling. Part I: theoretical model and simulation. Int J Adv Manuf Tech 20:631–638
14. Altintas Y (2000) Manufacturing automation: metal cutting mechanics, machine tool vibrations, and CNC design. Cambridge University Press, Cambridge
15. Gere JM, Timoshenko SP (1990) Mechanics of materials. PWS-Kent Publishing Company, Boston
16. Kivanc EB, Budak E (2004) Structural modeling of end mills for form error and stability analysis. Int J Mach Tools Manuf 44:1151–1161